Rapid Communications | Editors' Suggestion

Nontrivial scaling exponents of dislocation avalanches in microplasticity

G. Sparks and R. Maaß*

Department of Materials Science and Engineering and Frederick Seitz Materials Research Laboratory, University of Illinois at Urbana-Champaign, Urbana, Illinois 61801, USA

(Received 20 August 2018; published 5 December 2018)

Crystal plasticity causes structural fluctuations that can be scale-free and therefore admit power-law distributions. Numerous experiments, modeling, and theory have reported a scaling exponent that is in good agreement with mean-field predictions or a jamming-unjamming scenario. Via experiments on pure single crystals, we show here that the scaling exponent of a stress-integrated distribution for dislocation-avalanche sizes is nontrivial and can be in agreement with both models by admitting values between 1.0 and 2.3. This range is dictated by the structure and orientation of the deforming crystal, as long as the applied rate is below a critical value. For the highest symmetry tested, plastic strain can drive a change from truncated power-law scaling to pure exponential scaling. These findings show how the same crystal may yield different scaling exponents depending on intrinsic and extrinsic factors.

DOI: 10.1103/PhysRevMaterials.2.120601

In nature, many nonequilibrium systems exhibit power-law scaling of avalanche phenomena. Well-known examples are crackling-noise from earthquakes, magnetic domain-wall motion, or phase transformations [1]. In the past decades, signatures of scale-free probability distributions, P, have also been reported for plastic flow curves of crystals [2], dislocation structures [3], or surface-step patterns obtained after deformation [4]. One central aspect of these observations is that plasticity can lack a particular scale, which, for example, has been deduced from pure power-law scaling ($P \propto x^{-\tau}$) of acoustic emission pulse energies of creep in hexagonal close-packed ice crystals [5], or from pure power-law scaling of strain increments directly extracted from a stress-strain graph of uniaxially strained face-centered cubic (fcc) and body-centered cubic (bcc) crystals [6–8]. Importantly, these studies were in strong agreement on the obtained scaling exponent, τ, for event-energy or event-size distributions, which was found to be between 1.5 and 1.6. This numerical value is well in line with theoretical predictions from continuum and discrete dislocation models [9,10], and has prompted some studies to state that plasticity is a universal phenomenon that can be placed in the same "universality class" of other nonequilibrium systems with the same exponent [11–13]. Subsequent experiments and three-dimensional discrete dislocation dynamics (DDD) further support this view [12,14,15], but now report a truncated probability distribution of the form $P(S) \propto f(S) \times S^{-3/2}$, where S is the event size and $f(S)$ is some cutoff function that may depend on finite crystal sizes, stiffness, or hardening coefficient [12].

The seemingly consistent value of τ has lent support to mean-field models of avalanches near the depinning transition (MFD) [11,16], in which the predicted stress-binned probability density indeed scales as $P(S,\sigma) \propto S^{-3/2}$, whereas the stress-integrated distribution scales as $P_{\text{int}}(S) \propto S^{-2}$, which would have an exponent of -1 if represented by a complementary cumulative distribution function $C_{\text{int}}(S)$ (CCDF). Scaling collapses of binned data from both experiments and simulations [17–19] were found to match these predictions. Fundamentally, this suggests that the evolving dislocation network behaves as a stress-driven many-body system that interacts with a static pinning field. Here, an external stimulus (stress) acts as a control parameter that drives the system repeatedly to a pinning-depinning transition (yielding). At yield a critical point is reached, and a nonequilibrium phase transition triggers a dislocation avalanche. In the context of MFD, different distributions, such as $P(S,\sigma)$ or $P_{\text{int}}(S)$, also allow establishing links between their respective scaling exponents and other scaling relations, e.g. event size and event duration [20], but may require specific experimental conditions that cannot always be met.

In contrast to viewing yielding as a depinning transition, numerous DDD simulations have underlined the fact that yielding is a result of collective trapping [21,22], i.e., jamming, due to the formation of a complex network of interacting dislocations. This dynamic picture relies on collective dislocation interactions rather than a static pinning field and gives rise to a distinctly lower stress-resolved size scaling exponent of $\tau \approx 1$ [21,23] ($\tau \approx 1.3$, if stress integrated [23]). In addition, the jamming-unjamming mechanism has revealed that critical fluctuations take place over a larger range of control parameters, which shows that the system does not have a critical point, but is always close to criticality [22–25].

The matter of pinning-depinning vs jamming-unjamming remains debated, with some reports suggesting material-specific or size-specific exponents [26,27], which however do not reveal what fundamental parameters, or their combination, may determine a given value of τ. Hence, there is a strong lack of systematic experimental evidence obtained from realistic three-dimensional dislocation networks that potentially could conclude on the magnitude of τ and thereby on the dispute of pinning-depinning vs jamming-unjamming. We address this shortcoming and demonstrate how scaling exponents for the

*rmaass@illinois.edu

same crystal can admit exponents numerically compatible with both theories. Specifically, we focus on the effects of crystal orientation, drive rate, and deformation history on τ by deformation experiments of pure Nb (bcc) and Au (fcc) crystals.

We find that the scaling exponent, τ, for avalanche sizes increases systematically with increasing crystal symmetry in both Nb and Au, and its value for a given symmetry is distinctly higher in Nb than in Au. For a given lattice type, τ remains unaffected by drive rate as long as the applied deformation rate is below a critical rate $\dot{u}_{\mathrm{crit}}$, but this rate is two orders of magnitude lower in Nb than in Au. Prior plastic deformation via cold rolling does not significantly affect τ for deformation rates at or below $\dot{u}_{\mathrm{crit}}$, but shifts the power-law truncation to smaller avalanche sizes. It is furthermore demonstrated how a single-crystal system (bcc Nb) can exhibit truncated power-law scaling for a low-symmetry orientation, while for the highest symmetry it can develop toward a pure exponential avalanche distribution during deformation. This means the same material can experience a strain-dependent shift from one distribution to another. On the basis of these observations, we conclude that scaling exponents of microplasticity can admit numerical values encompassing both MFD and jamming-unjamming, not supporting the notion of a universal exponent.

We conduct microcrystal deformation experiments using a TI-950 nanoindentation platform. Precise details related to the experiments can be found in Refs. [28,29]. Nb and Au crystals of 2-μm diameter and a nominal height of 6 μm were produced via focused ion-beam milling. Four different loading-axis orientations ($\langle 123\rangle$, $\langle 011\rangle$, $\langle 111\rangle$, and $\langle 001\rangle$) were studied. The displacement rates $\dot{u}$ were varied between 0.06 and 600 nm/s for Nb and 6 and 6000 nm/s for Au, and all crystals were deformed to an engineering strain of ~ 0.2. The force-displacement data were analyzed with custom MATLAB codes, and determinations of the most suitable avalanche distributions and scaling exponents were done using the maximum likelihood estimator (MLE) method [30,31] (see Supplemental Material for details [32]). In the following, avalanche sizes are reported in axial displacement, whereas resolved shear stress, τ_{res}, and shear strain, γ, are used to quantify the plastic flow response.

The stress-integrated probability density distributions for Au are shown in Fig. 1(a) (see Fig. S1 in the Supplemental Material for equivalent plots for Nb [32]). The MLE-analysis shows that the data are best described with a truncated power law $P_{\mathrm{int}}(S) \propto e^{-\lambda S} \times S^{-\tau}$ and an orientation-dependent exponent (see Supplemental Material for details [32]): $\tau_{\mathrm{Au}\langle 123\rangle} = 1.01 \pm 0.02$, $\tau_{\mathrm{Au}\langle 011\rangle} = 1.22 \pm 0.08$, $\tau_{\mathrm{Au}\langle 111\rangle} = 1.95 \pm 0.07$, and $\tau_{\mathrm{Au}\langle 001\rangle} = 1.62 \pm 0.05$. From the MLE-analysis and the correspondingly obtained truncated power laws [fit lines in Fig. 1(a)], we construct $C_{\mathrm{int}}(S)$ via integration of $P_{\mathrm{int}}(S)$, obtaining $C_{\mathrm{int}}(S) \propto \Gamma(1-\tau, \lambda \times S)$, with Γ being the upper incomplete gamma function and λ a nonuniversal constant of the cutoff function $f(S)$. Subsequently, a least-squares method was used to find the best fit between the constructed $C_{\mathrm{int}}(S)$ curve (with the τ and λ values taken from the MLE analysis) and the experimental CCDF. This is shown in Fig. 1(b) for both Au and Nb, where the preference of $C_{\mathrm{int}}(S)$ over $P_{\mathrm{int}}(S)$ is motivated by the ability to present unbinned data. In the case

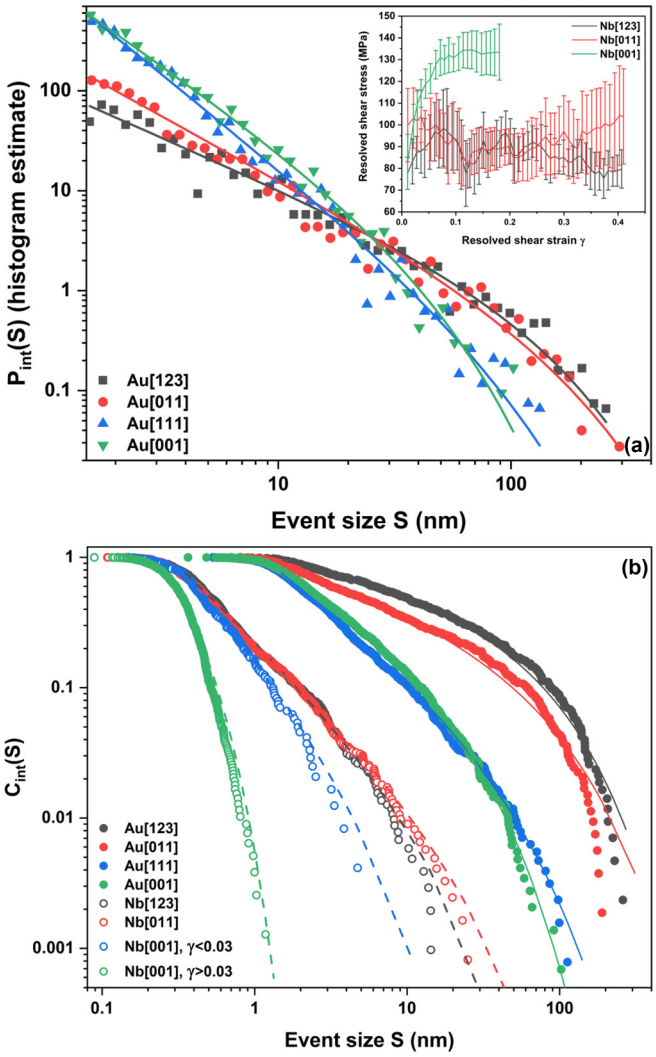

FIG. 1. (a) Probability density distribution $P_{\mathrm{int}}(S)$ for Au microcrystals of various orientations. The full lines are truncated power-law fits obtained from MLE analysis. The inset in (a) shows the resolved shear stress as a function of resolved shear strain for different orientations of Nb. Each curve is an average of 7–12 stress-strain curves. (b) $C_{\mathrm{int}}(S)$ constructed from (a) with corresponding truncated power-law fits for differently oriented Au- and Nb microcrystals. In the case of Nb$\langle 001\rangle$ for $\gamma > 0.03$, an exponential distribution fits the data best. $\dot{u}_{\mathrm{Au}} = 60$ nm/s and $\dot{u}_{\mathrm{Nb}} = 0.6$ nm/s.

of Nb, the same procedure was followed, with the particular difference that the highest symmetry loading axis ($\langle 001\rangle$) revealed a distinct change in flow response at low γ [see inset in Fig. 1(a); each curve is an average of seven or more flow curves], after which $d\tau_{\mathrm{res}}/d\gamma$ is equally low as for all other Nb orientations. The detailed analysis of the avalanche size distributions revealed a bimodal behavior, which changed at $\gamma = 0.03$. As a result, Fig. 1(b) displays two size distributions for Nb$\langle 001\rangle$, each for a different regime of γ. This led to the following $P_{\mathrm{int}}(S)$ scaling exponents (see Supplemental Material [32]): $\tau_{\mathrm{Nb}\langle 123\rangle} = 2.09 \pm 0.13$, $\tau_{\mathrm{Nb}\langle 011\rangle} = 2.07 \pm 0.08$, and $\tau_{\mathrm{Nb}\langle 001\rangle, \gamma < 0.03} = 2.23 \pm 0.22$, all of which are best described by a truncated power law. However, the best distribution for Nb$\langle 001\rangle$ and $\gamma > 0.03$ is of pure exponential form.

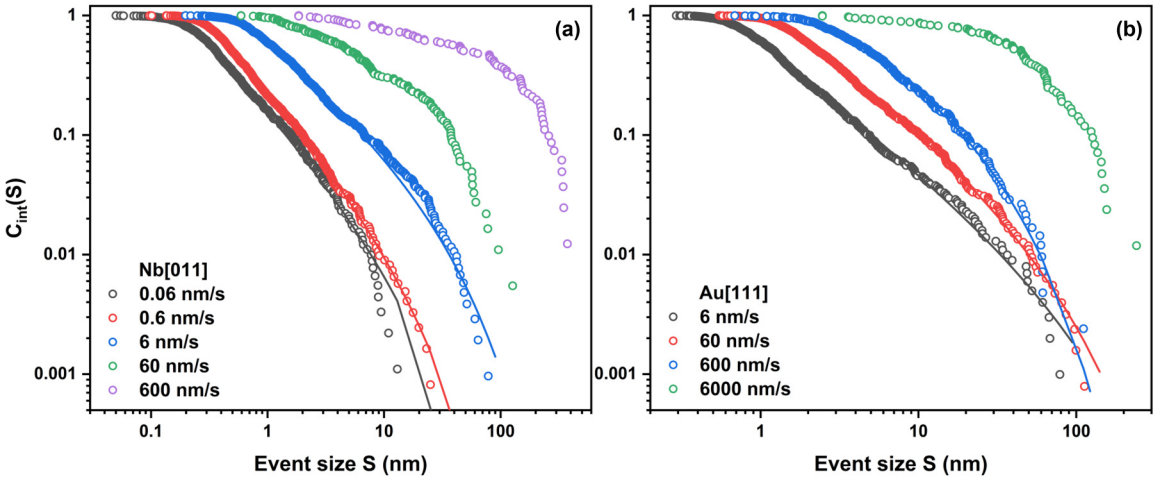

FIG. 2. $C_{int}(S)$ for Nb⟨011⟩ (a) and Au⟨111⟩ (b) as a function of applied displacement rate $\dot{u}$. Above a critical rate, $\dot{u}_{crit}$, the scaling exponent depends on $\dot{u}$. Full lines are truncated power-law fits.

Figure 1(b) demonstrates this increase in scaling exponent with symmetry via $C_{int}(S)$. The increase in τ is small between the one- and twofold symmetry, after which τ increases significantly for the three- and fourfold symmetry, which qualitatively agrees with results from phase-field modeling [33]. In the case of Au, the MLE analysis shows no strong trend away from a truncated power law as the most likely distribution, which can be quantified by the likelihood ratio, R, and the significance value, p. This is different for Nb, where in general these parameters less strongly favor a truncated power law, and where a strain-dependent type of statistics is observed for the fourfold symmetry. The latter shows that depending on strain, the power-law contribution can be lost entirely, transitioning the crystal into a system governed by pure exponential avalanche size statistics. This can be understood by the finite experimental resolution (∼0.25 nm) and a decreasing correlation length due to network evolution. As a result, one effectively only probes the largest events of the underlying distribution, which potentially is still of the truncated power-law type, but only the largest events can be resolved. Even though the distributions in Fig. 1(b) visibly display different scaling behavior, we emphasize that fitting a truncated power law with a fixed exponent, but a variable parameter in an exponential cutoff function, does not allow matching the experimental data. There is thus a marked influence of crystal orientation on the scaling exponent, where Au⟨111⟩, Nb⟨123⟩, and Nb⟨011⟩ are orientations that, within experimental uncertainties, may suggest agreement with MFD ($\tau = 2$), and the exponent value of Au⟨011⟩ may be seen as support for a jamming-unjamming picture ($\tau \approx 1.3$ [23]). We note that τ scales somewhat with $d\tau_{res}/d\gamma$ for Au, but that this is not the case for Nb. The cutoff values at $C_{int}(S) = 0.001$ for the different orientations reveal grouping into two main groups, one of which includes the ⟨123⟩- and ⟨011⟩ orientations, and the other one ⟨111⟩ and ⟨001⟩ (Au) or ⟨001⟩ (Nb). This trend matches the surface morphology of the deformed crystals that exhibits well-localized slip for the two lower symmetries, and well-distributed faint slip steps for the higher symmetries.

Since the structural fluctuations caused by the external drive have finite time scales, and in the case of crystal plasticity are thermally activated, it is possible to truncate the avalanche size distribution at the lower size end when drive conditions are not sufficiently slow (close to the adiabatic limit). This could generally reduce the size-scaling exponent if the underlying avalanche dynamics is of similar timescale as the drive. For each crystal system studied, it is thus of importance to precisely determine at which external drive rate, $\dot{u}_{crit}$, this occurs. Following the identical procedure as for the data in Fig. 1, we find that $P_{int}(S)$ for different applied rates for both Nb⟨011⟩ and Au⟨111⟩ are truncated power-laws: $\tau_{Nb\langle011\rangle,\ 0.06\ nm/s} = 2.09 \pm 0.04$, $\tau_{Nb\langle011\rangle,\ 0.6\ nm/s} = 2.07 \pm 0.08$, $\tau_{Nb\langle011\rangle,6\ nm/s} = 1.80 \pm 0.05$, and $\tau_{Au\langle111\rangle,6\ nm/s} = 2.02 \pm 0.05$, $\tau_{Au\langle111\rangle,60\ nm/s} = 1.95 \pm 0.07$, $\tau_{Au\langle111\rangle,600\ nm/s} = 1.53 \pm 0.19$. Figure 2 summarizes $C_{int}(S)$ for these distributions. For the higher rates, no valid truncated power law could be identified. It is thus found that $\dot{u}_{crit}$ is as low as 0.6 nm/s in the case of Nb, and 60 nm/s in the case of Au, in order to not affect τ. These results are independent of orientation, which we will comment on further in relation to Fig. 3. Given the data in Fig. 2, $\dot{u}_{crit}$ thus needs

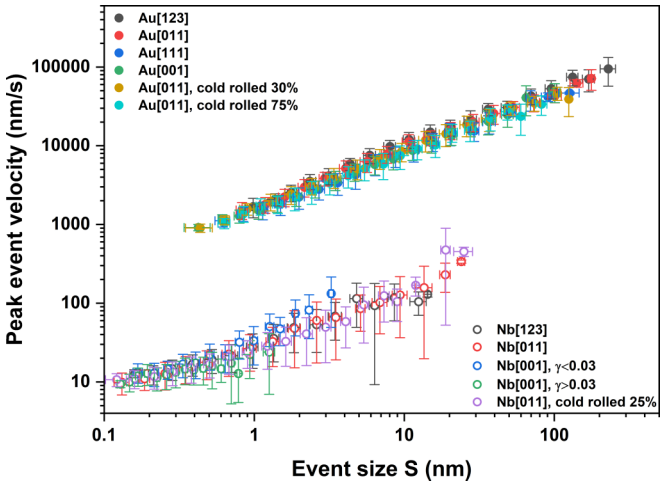

FIG. 3. Avalanche peak velocity as a function of avalanche size for Au and Nb of various orientations, and cold-rolled Au⟨011⟩ and Nb⟨011⟩. All data were obtained at $\dot{u}_{crit}$.

to be quantified for each studied material prior to concluding on the numerical value of τ. By increasing $\dot{u}$, the distributions lose a growing fraction of their smaller avalanches, pushing $C_{\text{int}}(S)$ to the higher event sizes and reducing the exponent, eventually erasing the scaling.

While the effect of applied rate (external drive velocity) has been touched on in the literature [17,34], the data in Fig. 2 demonstrate the importance of finding $\dot{u}_{\text{crit}}$, which from an experimental perspective is an unexpectedly low rate for Nb. These constraints will become increasingly severe at larger sample sizes, because typical deformation experiments are based on strain-rate constancy rather than maintaining a constant absolute displacement rate.

An extraction of the peak-event velocity from the time-resolved velocity profiles [35] for all orientations reveals a very systematic scaling of type $\langle v\rangle \sim \langle S\rangle^{\alpha}$, where $\langle v\rangle$ is the average peak velocity and $\langle S\rangle$ the average event size for that bin. Such scaling has to our knowledge only been predicted by MFD ($\alpha = 0.5$) [36]. In the present work, the emphasis lies on the fact that at $\dot{u}_{\text{crit}}$ orientation does not affect α, but material does ($\alpha_{\text{Au}} = 0.73 \pm 0.06$; $\alpha_{\text{Nb}} = 0.66 \pm 0.16$). At $\dot{u} > \dot{u}_{\text{crit}}$, α decreases with increasing rate. More importantly, and in relation to the findings of Fig. 2, one can conclude that, within the experimental resolution, it is the low velocity of the smallest avalanches that sets $\dot{u}_{\text{crit}}$. In both cases, the ratio $\langle v\rangle_{min}/\dot{u}_{\text{crit}} \approx 160 \pm 40$, depending on the scatter bounds. Figure 3 also reveals that the velocity-size scaling remains the same across all orientations and shear strains. Instead, the only offsetting factor is the lattice type, which manifests itself in a reduced avalanche velocity for Nb that can be understood on the basis of rate-limiting screw dislocation activity during the avalanche. Since events of all sizes can occur at any γ, Fig. 3 furthermore shows that any increase in dislocation density during flow does not change the velocity-size scaling, i.e., the avalanche dynamics seems insensitive to network evolution in the tested crystals. This is most prominently shown with Au⟨111⟩, which has a distinctly higher hardening rate than the other orientations (see Supplemental Material [32]), but yet α is identical.

The insensitivity of the avalanche velocity-size scaling to the dislocation network can further be demonstrated on the basis of predeformation of the same original crystals. To this end, we cold rolled Nb⟨011⟩ to 25%, and Au⟨011⟩ to 30% and 75% thickness reduction, respectively. This amount of cold rolling is known to introduce a dislocation substructure corresponding to stage II or III hardening [37,38]. The size-velocity data are in all cases indistinguishable in comparison to the as-received well-annealed crystals. The truncated power-law scaling exponent of $P_{\text{int}}(S)$ for the cold-rolled crystal conditions are $\tau_{\text{Nb}\langle 011\rangle,25\%\text{ rolled}} = 1.95 \pm 0.06$, $\tau_{\text{Au}\langle 011\rangle,30\%\text{ rolled}} = 1.27 \pm 0.07$, and $\tau_{\text{Au}\langle 011\rangle,75\%\text{ rolled}} = 1.23 \pm 0.07$ for which $C_{\text{int}}(S)$ is shown in Fig. 4. These exponents are within the error bar of the as-grown crystals, but a clear increase of the exponential truncation $e^{-\lambda S}$ is observed, underlining how large avalanches are increasingly suppressed by the increased network entanglement and substructure formation. This finding is somewhat different than previously proposed [39], where $P_{\text{int}}(S)$ was found unaffected by predeformation to the onset of stage III hardening. We note that the subtle change of $C_{\text{int}}(S)$ for Nb⟨011⟩ is visibly indistinguishable in $P_{\text{int}}(S)$,

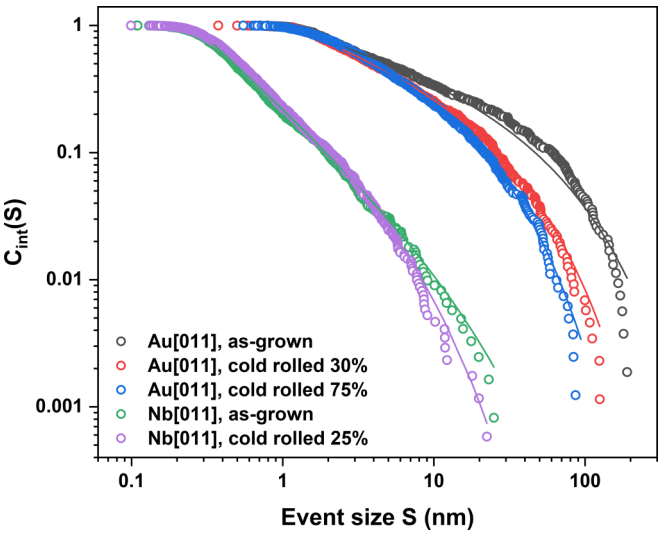

FIG. 4. $C_{\text{int}}(S)$ for Au⟨111⟩ and Nb⟨011⟩ after cold rolling, revealing identical scaling exponents, but increasing dominance of the exponential truncation. All data were obtained at $\dot{u}_{\text{crit}}$.

likely due to the involved binning procedure. In stark contrast to the orientation dependence displayed in Fig. 1, where a true change in τ is seen, the apparent slope change in Fig. 4 due to prestraining is only due to amplified power-law truncation. It is thus crystal orientation that determines τ for $\dot{u} \leqslant \dot{u}_{\text{crit}}$, but not the preexisting dislocation network, as long as power-law fluctuations are admitted and the pure exponential regime has not been reached.

The above experimental study on pure single fcc- and bcc microcrystals reveals that the scaling exponent for event-size distribution of intermittent plastic flow varies significantly in a material-orientation-rate parameter space, which puts earlier experimental studies in a different perspective. Indeed, one has to reassess to what degree previously reported agreements with MFD are robust against the variations shown here. Since the jamming-unjamming picture has *per se* no predefined exponents, it needs to be seen to which degree compatibility is found with the experimentally revealed nontrivial exponents. Since some of the here-revealed changes of τ are not due to truncation effects that may be classified as experimentally tunable (tuned criticality [17]) our results indicate that fluctuations in crystal plasticity are not universally described by the same exponent. Furthermore, it is possible to obtain an arbitrary exponent by a combination of a given orientation and a rate larger than the critical rate.

The overall range of exponents could be framed within a picture where crystal symmetry drives a transition from a jamming-dominated ensemble to a pinning-dominated ensemble, by an increasing density of sessile segments originating from initial slip-system interaction. Such a scenario raises the question as to why the lower-symmetry Nb crystals already have scaling exponents numerically representative of MFD, thereby excluding a jamming-unjamming mechanism. This can be reconciled by the fact that boundary conditions in microcrystal deformation are known to trigger deformation on additional slip systems than geometrically predicted [40]. Considering only the primary and conjugate slip planes and

one active slip direction per plane, it is straightforward to show that a bcc crystal oriented for single slip has initially six interacting slip systems available, which already exceeds the number available to the highest symmetry fcc crystal. Correspondingly, if at sufficiently slow driving rate, slip system interaction is determining τ, the active number of them give room for both MFD and jamming-unjamming. Since this picture requires the precise knowledge and details on the evolving dislocation structure as to verify the symmetry-driven development of an effective pinning field, only realistic three-dimensional DDD simulations will allow scrutinizing this proposition.

Deformation of crystals having highly mobile dislocations that exhibited scale-free behavior has also motivated attributing self-organized critical (SOC) behavior to plasticity [6]. This concept describes a dynamical system that arranges itself such that it always is at a critical point [41]. One of the important properties of SOC behavior is that it is self-similar or scale-free. The fact that the same type of crystal (here Nb) can admit fluctuations that are best described by a truncated power law at low strains, but subsequently transitions to pure exponential fluctuations, suggests, at least within the experimental resolution, that the crystal transitions into a state of network entanglement for which SOC behavior may no longer be applicable.

This study reveals the large range of scaling exponents that plasticity in pure crystals may admit, therefore shedding light onto inconsistent data in the literature and highlighting the need to carefully examine under which conditions reliable comparisons between scaling exponents can be made. Such efforts are critically needed in order to exploit statistical properties of evolving dislocation ensembles in order to incorporate the physics of groups of dislocations into novel macroscopic deformation models.

The authors thank P. M. Derlet, D. M. Dimiduk, K. A. Dahmen, P. D. Ispanovity, and A. J. Beaudoin for fruitful discussions. This research was carried out in part in the Frederick Seitz Materials Research Laboratory Central Research Facilities, University of Illinois. R.M. is grateful for financial support by the NSF CAREER program (Grant No. NSF DMR 1654065), and for start-up funds provided by the Department of Materials Science and Engineering at University of Illinois at Urbana-Champaign.

[1] J. P. Sethna, K. A. Dahmen, and C. R. Myers, Nature (London) **410**, 242 (2001).
[2] M. D. Uchic, D. M. Dimiduk, J. N. Florando, and W. D. Nix, Science, **305**, 986 (2004).
[3] P. Hähner, K. Bay, and M. Zaiser, Phys. Rev. Lett. **81**, 2470 (1998).
[4] M. Zaiser, F. M. Grasset, V. Koutsos, and E. C. Aifantis, Phys. Rev. Lett. **93**, 195507 (2004).
[5] M. C. Miguel, A. Vespignani, S. Zapperi, J. Weiss, and J. R. Grasso, Nature (London) **410**, 667 (2001).
[6] D. M. Dimiduk, C. Woodward, R. LeSar, and M. D. Uchic, Science **312**, 1188 (2006).
[7] M. Zaiser, J. Schwerdtfeger, A. S. Schneider, C. P. Frick, B. G. Clark, P. A. Gruber, and E. Arzt, Philos. Mag. **88**, 3861 (2008).
[8] B. Devincre, T. Hoc, and L. Kubin, Science **320**, 1745 (2008).
[9] M. Zaiser, Adv. Phys. **55**, 185 (2006).
[10] M. Zaiser and P. Moretti, J. Stat. Mech. (2005) P08004.
[11] J. T. Uhl, S. Pathak, D. Schorlemmer, X. Liu, R. Swindeman, B. A. W. Brinkman, M. LeBlanc, G. Tsekenis, N. Friedman, R. Behringer, D. Denisov, P. Schall, X. Gu, W. J. Wright, T. Hufnagel, A. Jennings, J. R. Greer, P. K. Liaw, T. Becker, G. Dresen, and K. A. Dahmen, Sci. Rep. **5**, 16493 (2015).
[12] F. F. Csikor, C. Motz, D. Weygand, M. Zaiser, and S. Zapperi, Science **318**, 251 (2007).
[13] A. S. Argon, Philos. Mag. **93**, 3795 (2013).
[14] S. Brinckmann, J.-Y. Kim, and J. R. Greer, Phys. Rev. Lett. **100**, 155502 (2008).
[15] B. Devincre and L. Kubin, C. R. Phys. **11**, 274 (2010).
[16] K. A. Dahmen, Y. Ben-Zion, and J. T. Uhl, Phys. Rev. Lett. **102**, 175501 (2009).
[17] N. Friedman, A. T. Jennings, G. Tsekenis, J.-Y. Kim, M. Tao, J. T. Uhl, J. R. Greer, and K. A. Dahmen, Phys. Rev. Lett. **109**, 095507 (2012).
[18] R. Maaß, M. Wraith, J. T. Uhl, J. R. Greer, and K. A. Dahmen, Phys. Rev. E **91**, 042403 (2015).
[19] P. M. Derlet and R. Maass, Model. Simul. Mater. Sci. Eng. **21**, 035007 (2013).
[20] D. Gianfranco and Z. Stefano, J. Stat. Mech. (2006) P01002.
[21] M. J. Alava, L. Laurson, and S. Zapperi, Eur. Phys. J.: Spec. Top. **223**, 2353 (2014).
[22] M. Ovaska, A. Lehtinen, M. J. Alava, L. Laurson, and S. Zapperi, Phys. Rev. Lett. **119**, 265501 (2017).
[23] P. D. Ispánovity, L. Laurson, M. Zaiser, I. Groma, S. Zapperi, and M. J. Alava, Phys. Rev. Lett. **112**, 235501 (2014).
[24] A. Lehtinen, G. Costantini, M. J. Alava, S. Zapperi, and L. Laurson, Phys. Rev. B **94**, 064101 (2016).
[25] P. D. Ispánovity, I. Groma, G. Gyöergyi, P. Szabó, and W. Hoffelner, Phys. Rev. Lett. **107**, 085506 (2011).
[26] J. Weiss, W. B. Rhouma, T. Richeton, S. Dechanel, F. Louchet, and L. Truskinovsky, Phys. Rev. Lett. **114**, 105504 (2015).
[27] P. Zhang, O. U. Salman, J.-Y. Zhang, G. Liu, J. Weiss, L. Truskinovsky, and J. Sun, Acta Mater. **128**, 351 (2017).
[28] R. Maass, P. M. Derlet, and J. R. Greer, Small **11**, 341 (2015).
[29] G. Sparks, P. S. Phani, U. Hangen, and R. Maass, Acta Mater. **122**, 109 (2017).
[30] J. Alstott, E. Bullmore, and D. Plenz, PLoS One **9**, e85777 (2014).
[31] A. Clauset, C. R. Shalizi, and M. E. J. Newman, SIAM Rev. **51**, 661 (2009).
[32] See Supplemental Material at http://link.aps.org/supplemental/10.1103/PhysRevMaterials.2.120601 for details on the MLE analysis.

[33] P. Biscari, M. F. Urbano, A. Zanzottera, and G. Zanzotto, J. Elasticity **123**, 85 (2016).
[34] S. Papanikolaou, D. M. Dimiduk, W. Choi, J. P. Sethna, M. D. Uchic, C. F. Woodward, and S. Zapperi, Nature (London) **490**, 517 (2012).
[35] G. Sparks and R. Maass, Acta Mater. **152**, 86 (2018).
[36] M. LeBlanc, L. Angheluta, K. Dahmen, and N. Goldenfeld, Phys. Rev. E **87**, 022126 (2013).
[37] G. Taylor and J. W. Christian, Phil. Mag. **15**, 893 (1967) .
[38] J. W. Steeds, Proc. R. Soc. London, Ser. A **292**, 343 (1966).
[39] R. Maass and P. M. Derlet, Acta Mater. **143**, 338 (2018).
[40] R. Maass and M. D. Uchic, Acta Mater. **60**, 1027 (2012).
[41] P. Bak, C. Tang, and K. Wiesenfeld, Phys. Rev. Lett. **59**, 381 (1987).